

Pushing Toward the Simplex Vertices: A Simple Remedy for Code Collapse in Smoothed Vector Quantization

Takashi Morita^{*1,2}

¹Academy of Emerging Sciences, Chubu University

²Institute for Advanced Research, Nagoya University

January 30, 2026

Abstract

Vector quantization, which discretizes a continuous vector space into a finite set of representative vectors (a *codebook*), has been widely adopted in modern machine learning. Despite its effectiveness, vector quantization poses a fundamental challenge: the non-differentiable quantization step blocks gradient backpropagation. *Smoothed* vector quantization addresses this issue by relaxing the hard assignment of a codebook vector into a weighted combination of codebook entries, represented as the matrix product of a simplex vector and the codebook. Effective smoothing requires two properties: (1) smoothed quantizers should remain close to a onehot vector, ensuring tight approximation, and (2) all codebook entries should be utilized, preventing *code collapse*. Existing methods typically address these desiderata separately. By contrast, the present study introduces a simple and intuitive regularization that promotes both simultaneously by minimizing the distance between each simplex vertex and its K -nearest smoothed quantizers. Experiments on representative benchmarks—including discrete image autoencoding and contrastive speech representation learning—demonstrate that the proposed method achieves more reliable codebook utilization and improves performance compared to prior approaches.

1 Introduction

Vector quantization is a method for discretizing a continuous vector space (Gray, 1984; van den Oord et al., 2017). It maps each vector in the continuous space to the nearest element of a finite set of representative vectors (a.k.a. a *codebook*). The resulting discrete representations are easier to manipulate and interpret than the original continuous forms, and have proven effective across diverse applications, including image generation (Esser et al., 2021; Ramesh et al., 2021; Rombach et al., 2022; Yu et al., 2022b), speech recognition (Baevski et al., 2020a,b), and music generation (Hadjeres and Crestel, 2020; Dhariwal et al., 2020).

When integrated into deep neural networks, however, vector quantization introduces a fundamental challenge: quantization is a non-differentiable operation that blocks gradient backpropagation (van den Oord et al., 2017). Accordingly, some approximation is required to enable learning through quantization.

One effective workaround is to *smooth* vector quantization (Jang et al., 2017). The selection of a codebook vector can be expressed as multiplying the codebook matrix by its corresponding onehot vector $(0, \dots, 1, \dots, 0)^\top$, whose nonzero entry indexes the chosen vector. *Smoothed* vector quantization relaxes this onehot vector to lie within the simplex $\Delta^{M-1} := \{(p_1, \dots, p_M) \mid \sum_{m=1}^M p_m = 1\}$, where M denotes the number of codebook vectors. Consequently, differentiable mappings (e.g., softmax) become available and can be incorporated into neural networks.

To successfully approximate onehot quantizers, smoothed quantizers must be distributed around the vertices of the simplex (orange “o” in Figure 1A). At the same time, they should not concentrate around a few vertices, leaving other codebook entries unused (blue “x”). This latter issue—called *code collapse*—has been identified as a major challenge in vector quantization (Dieleman et al., 2018; Baevski et al., 2020b; Dhariwal et al., 2020; Fifty et al., 2025). A widely adopted workaround for code collapse (in smoothed quantization) is to introduce an auxiliary learning objective that maximizes the entropy or perplexity of the *mean* of the smoothed quantizers (Dieleman et al., 2018; Baevski et al., 2020b, see §2.3 for the

^{*}tmorita@alum.mit.edu

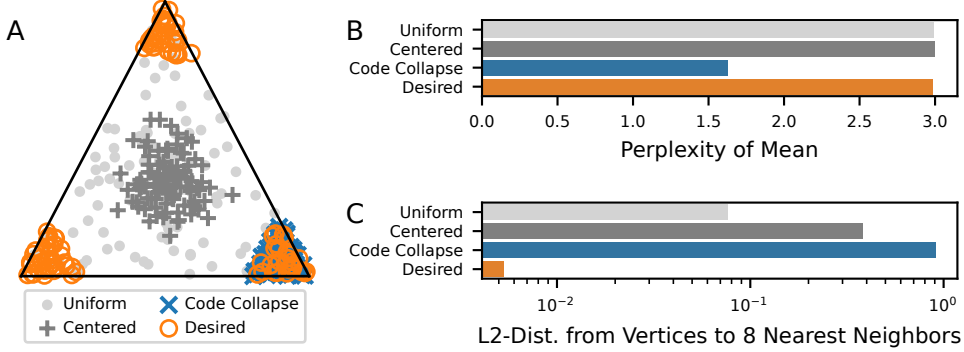


Figure 1: (A) Four different distributions on the simplex Δ^{3-1} . For effective smoothed vector quantization, samples should be concentrated near the vertices of the simplex (i.e., onehot-like vectors; orange), rather than centered (dark gray) or uniformly spread across the simplex (light gray). At the same time, each vertex must be neighbored by some samples to avoid code collapse (blue). (B) Maximizing the perplexity of the sample mean (Baevski et al., 2020b) penalizes code collapse but cannot discriminate among the other three distributions. (C) The proposed K -nearest neighbor (KNN) distance minimization ($K = 8$) favors the desired vertex-concentrated distribution while also preventing code collapse.

formal definition). However, maximizing the entropy/perplexity of the mean can be achieved by various distributions, not only the desired vertex-neighboring ones. For example, both uniform and center-concentrated distributions have their mean at the simplex center (Figure 1A), which also maximizes this objective (Figure 1B). Accordingly, an additional mechanism is needed to tighten the smoothing (e.g., by adjusting the temperature parameter of the (Gumbel-)softmax; see §2.2).

Beyond this standard approach, however, there exists a simple and unified strategy for simultaneously tightening smoothed quantization and maximizing codebook usage: *Why don't we directly encourage clustering around all simplex vertices?* Specifically, minimizing the distance between each simplex vertex and its K -nearest neighbors (KNNs) satisfies both desiderata at once (Figure 1C). The present study investigates this intuitive yet underexplored approach, comparing it against existing alternatives on representative benchmarks. The results indicate that the proposed method enables the exhaustive usage of the entire codebook, even when other approaches suffer from code collapse.

The contributions of this work are summarized as follows:

- Neural vector quantization is reformulated as a smoothing problem of onehot vectors. This simple reformulation has been absent in the literature, which traditionally framed vector quantization as an extension of variational autoencoding (Kingma and Welling, 2014; Jang et al., 2017; van den Oord et al., 2017).
- Under this reformulation, an effective regularization loss function is proposed to promote both tight smoothing and exhaustive code utilization. The method demonstrates robustness across different learning settings.

The remainder of this paper is organized as follows. §2 reviews related studies on vector quantization. §3 introduces the proposed method, which is then evaluated on representative benchmarks in §4. Finally, §5 discusses the results and the limitations of the proposed method.

2 Related Studies

The central challenge of vector quantization lies in its non-differentiability, which disrupts the backpropagation of gradients in neural networks. To address this, either the gradient computation (backward path) or the quantization itself (forward path) must be approximated.

2.1 Approximation in the Backward Path (Gradient Estimation)

One line of work retains the original non-differentiable quantization in the forward path but replaces the gradient computation in the backward path. Let $\mathbf{z} \in \mathbf{R}^D$ denote a pre-quantized feature vector, and $\{\mathbf{q}_1, \dots, \mathbf{q}_M\} \subset \mathbf{R}^D$ the set of quantized

vectors. Quantization maps \mathbf{z} to its “closest” codebook entry according under a distance metric \mathcal{D} : i.e., $\mathbf{z} \mapsto \mathbf{q}_{\iota(\mathbf{z})}$ where $\iota(\mathbf{z}) := \operatorname{argmin}_m \mathcal{D}(\mathbf{z}, \mathbf{q}_m)$. Consequently, the partial derivatives $\frac{\partial q_{\iota(\cdot),i}}{\partial z_j}$ are ill-defined and must be approximated.

A canonical approximation—known as the *straight-through estimation* (STE)—replaces the ill-defined Jacobian with the identity matrix (van den Oord et al., 2017):

$$\frac{\partial q_{\iota(\cdot),i}}{\partial z_j} \approx \begin{cases} 1 & i = j \\ 0 & \text{otherwise} \end{cases} \quad (1)$$

Algorithmically, the STE is implemented using the `detach` operation, which excludes its argument from gradient computation:

$$\text{STE}(\mathbf{q}_{\iota(\mathbf{z})}, \mathbf{z}) := \mathbf{q}_{\iota(\mathbf{z})} + \mathbf{z} - \text{detach}(\mathbf{z}) \quad (2)$$

Here, $\mathbf{z} - \text{detach}(\mathbf{z})$ evaluates to zero, while the gradient with respect to \mathbf{z} can still be propagated through the first term.

More recently, Fifty et al. (2025) proposed an alternative gradient approximation, and demonstrated its empirical superiority over the STE:

$$\text{RE}(\mathbf{q}_{\iota(\mathbf{z})}, \mathbf{z}) := \text{detach} \left(\frac{\|\mathbf{q}_{\iota(\mathbf{z})}\|}{\|\mathbf{z}\|} \mathbf{R} \right) \mathbf{z} \quad (3)$$

where \mathbf{R} is the rotation matrix aligning \mathbf{z} to $\mathbf{q}_{\iota(\mathbf{z})}$,¹ and $\frac{\|\mathbf{q}_{\iota(\mathbf{z})}\|}{\|\mathbf{z}\|}$ rescales the rotated vector to match the amplitude of $\mathbf{q}_{\iota(\mathbf{z})}$. In this formulation, the Jacobian of the quantization is approximated by the scaled rotation matrix:

$$\frac{\partial q_{\iota(\cdot),i}}{\partial z_j} \approx \frac{\|\mathbf{q}_{\iota(\mathbf{z})}\|}{\|\mathbf{z}\|} \mathbf{R} \quad (4)$$

2.2 Approximation in the Forward Path (Smoothing)

An alternative approach approximates the forward quantization itself. Using the onehot representation \mathbf{e}_m of the code index m , quantization can be expressed as:

$$\mathbf{q}_{\iota(\mathbf{z})} = \mathbf{Q} \mathbf{e}_{\iota(\mathbf{z})} \quad (5)$$

where $\mathbf{Q} := (\mathbf{q}_1, \dots, \mathbf{q}_M)$. *Smoothed* quantization extends the possible range of \mathbf{e}_m to the simplex Δ^{M-1} . As noted in §1, effective learning requires smoothed quantizers $\mathbf{p} \in \Delta^{M-1}$ to concentrate near the vertices of the simplex (i.e., $\mathbf{p} \approx \mathbf{e}_m$ for some m).

A widely studied instance of smoothed quantization is Gumbel-softmax sampling (Jang et al., 2017). Given assignment probabilities π_m of \mathbf{z} to the m -th code—typically log-proportional to their dot-product $\mathbf{q}_m^\top \mathbf{z}$ —categorical sampling can be implemented using Gumbel samples $g_m = -\log(-\log u_m)$ with $u_m \sim \text{Uniform}(0, 1)$:

$$\begin{aligned} \iota(\mathbf{z}) &\sim \text{Categorical}(\pi_1, \dots, \pi_M) \\ \Leftrightarrow \iota(\mathbf{z}) &= \operatorname{argmax}_m (g_m + \log \pi_m) \end{aligned} \quad (6)$$

Replacing `argmax` above with `softmax` yields a smoothed quantization:

$$p_m = \frac{\exp((g_m + \log \pi_m) / \tau)}{\sum_{m'} \exp((g_{m'} + \log \pi_{m'}) / \tau)} \quad (7)$$

where lowering the temperature parameter τ produces a tighter approximation of categorical sampling.

The Gumbel-softmax sampling can also be combined with hard quantization using the STE:

$$\text{STE}(\mathbf{e}_{\iota(\mathbf{z})}, \mathbf{p}) = \mathbf{e}_{\iota(\mathbf{z})} + \mathbf{p} - \text{detach}(\mathbf{p}) \quad (8)$$

¹The rotation matrix is given by $\mathbf{R} = \mathbf{I} - 2\hat{\mathbf{v}}\hat{\mathbf{r}}^\top + 2\hat{\mathbf{q}}_{\iota(\mathbf{z})}\hat{\mathbf{z}}^\top$, where $\hat{\mathbf{v}} := \mathbf{v}/\|\mathbf{v}\|$ is the L2-normalization of vector \mathbf{v} , and $\mathbf{r} := \hat{\mathbf{q}}_{\iota(\mathbf{z})} + \hat{\mathbf{z}}$.

2.3 Regularization

Beyond approximation strategies, vector quantization also requires auxiliary regularization losses to ensure effective training. For example, the STE alone does not guarantee alignment between pre-quantized features and codebook entries. This alignment is instead fostered by the following regularization loss, \mathcal{L}_{reg} (van den Oord et al., 2017; Fifty et al., 2025):

$$\mathcal{L}_{\text{total}} = \mathcal{L}_{\text{main}} + \mathcal{L}_{\text{reg}} \quad (9)$$

$$\mathcal{L}_{\text{reg}} = \mathcal{L}_{\text{hard}}$$

$$\begin{aligned} &:= N^{-1} \sum_{i=1}^N \left(\underbrace{\beta \|\mathbf{z}_i - \text{detach}(\mathbf{q}_{\iota(\mathbf{z}_i)})\|^2}_{\text{Commitment Loss}} \right. \\ &\quad \left. + \underbrace{\|\text{detach}(\mathbf{z}_i) - \mathbf{q}_{\iota(\mathbf{z}_i)}\|^2}_{\text{Codebook Loss}} \right) \end{aligned} \quad (10)$$

where $\mathcal{L}_{\text{main}}$ is the primary task loss (e.g., L2 regression in autoencoding), and $\beta > 0$ is a weighting hyperparameter. As defined in Equation 10, $\mathcal{L}_{\text{hard}}$ consists of two components. The first term (known as the *commitment loss*) aligns each pre-quantized feature \mathbf{z}_i in a batch ($i = 1, \dots, N$) with their nearest codebook entry $\mathbf{q}_{\iota(\mathbf{z}_i)}$. The second term (called the *codebook loss*) moves each codebook vector \mathbf{q}_m toward the centroid of its assigned features whose nearest neighbor is \mathbf{q}_m (i.e., $\{\mathbf{z}_i : \iota(\mathbf{z}_i) = m\}$).

It should be noted, however, that the codebook loss in Equation 10 does not inherently prevent code collapse. Some codebook vectors may never serve as the nearest neighbor of any pre-quantized feature and therefore receive no updates (Zhu et al., 2025). Accordingly, previous studies have resorted to additional workarounds; for example, unused codebook vectors may be reset to the positions of pre-quantized features (Dhariwal et al., 2020). More recently, Zhu et al. (2025) proposed another remedy called *SimVQ*, which reparameterizes the codebook Q as the product of a randomly frozen matrix $Q' \in \mathbb{R}^{M \times D}$ and a learnable matrix $W \in \mathbb{R}^{D \times D}$ (i.e., $Q = Q'W$). In this formulation, all codebook vectors share learnable parameters with one another ($\mathbf{q}_m = q'_{m,1}\mathbf{w}_1 + \dots + q'_{m,D}\mathbf{w}_D$), so updates to one vector propagate to the others.

Similarly, smoothed quantization also requires auxiliary regularization to avoid code collapse. A widely adopted option is the normalized perplexity of the mean assignment probability (Dieleman et al., 2018; Baevski et al., 2020b):

$$\mathcal{L}_{\text{reg}} = \mathcal{L}_{\text{ppl}} := \frac{\exp(-\sum_m \bar{\pi}_m \log \bar{\pi}_m)}{M} \quad (11)$$

$$\bar{\pi}_m := N^{-1} \sum_{i=1}^N \pi_{i,m} \quad (12)$$

As noted in §1, this perplexity-based regularization does not promote the onehotness of π_i , failing to distinguish onehot-like samples from uniform or centered ones (Figure 1B). Onehotness can instead be induced by annealing the temperature parameter of the Gumbel-softmax sampling ($\tau \rightarrow 0$). However, manually scheduling this annealing is empirically challenging. The next section therefore proposes an alternative regularization loss that automatically encourages onehotness within the framework of gradient-based learning, while simultaneously preventing code collapse.

3 Methods

As noted in previous sections, ideal smoothed quantizers $\mathbf{p} \in \Delta^{M-1}$ are distributed near the vertices of the simplex (Figure 1A). Moreover, each vertex should have at least some smoothed quantizers in its neighborhood; otherwise, the quantization suffers from code collapse. A simple way to achieve these objectives simultaneously is to impose a loss penalizing the deviation of the KNNs from each vertex (Figure 1C):

$$\mathcal{L}_{\text{reg}} = \mathcal{L}_{\text{KNN}} := (MK)^{-1} \sum_{m=1}^M \sum_{k=1}^K \mathcal{D}(\mathbf{e}_m, \mathbf{p}^{(m,k)}) \quad (13)$$

where $\mathbf{p}^{(m,k)}$ denotes the k -th nearest neighbor of the simplex vertex (onehot vector) \mathbf{e}_m according to a distance/deviation metric \mathcal{D} . Two options for \mathcal{D} are considered in this study: the squared L2 distance, $\|\mathbf{e}_m - \mathbf{p}^{(m,k)}\|^2$, and cross-entropy, $-\log p_m^{(m,k)}$.

At first glance, the proposed regularization may appear similar to the commitment and codebook losses used in the gradient-estimation approaches (Equation 10). Both involve nearest neighbors, but the two methods differ in their choice of anchors and neighbors. While commitment and codebook losses take data points as anchors and identify their nearest codebook entries, the proposed method uses codebook entries as anchors and treats data as neighbors. Accordingly, the proposed regularization ensures that every codebook entry receives optimization feedback, whereas commitment/codebook losses may leave some entries untrained if they never become the nearest neighbor of any data point.

A further advantage of the proposed regularization is that Gumbel-softmax sampling is no longer required; smoothed quantizers can be obtained directly as $\mathbf{p} = \pi = \text{softmax}(Q^\top \mathbf{z})$.² At the same time, the proposed regularization is fully compatible with Gumbel-softmax sampling; one can simply replace \mathbf{p} (Gumbel-softmax samples) in Equation 13 with π (assignment probabilities).

During inference, hard quantization is applied by taking $\text{argmax}_m p_m$ in the onehot representation. In the following section, both the deterministic and stochastic approaches are evaluated on representative benchmarks.

4 Experiments

The proposed regularization for smoothed vector quantization was benchmarked on two tasks: discrete autoencoding (§4.1) and contrastive learning (§4.2). The Python code used for these experiments will be published once this study is accepted.

4.1 Discrete Autoencoding

The first benchmark assessed the proposed regularization in the context of discrete autoencoding on the ImageNet dataset (Deng et al., 2009). Input images were convolutionally encoded into latent feature maps, whose pixels were subsequently quantized (Esser et al., 2021; Fifty et al., 2025). A decoder convolutional network reconstructed the input images from these quantized feature maps, and the entire model was trained to minimize the L2 reconstruction loss (L_{main} in Equation 9). Further details of the network architecture and training setup are provided in Appendix B.1.

Extending prior work (Esser et al., 2021; Fifty et al., 2025), four combinations of feature map and codebook sizes were examined. In addition to the previously studied configurations of $H \times W \times C = 16 \times 16 \times 32$ ($M = 1024$) and $64 \times 64 \times 3$ ($M = 8196$), the channel dimensionality of the latter was further increased to $C = 32$ and $C = 2048$, yielding feature maps of size $64 \times 64 \times 32$ and $64 \times 64 \times 2048$ (both with $M = 8196$).

Each model was trained using four GPUs in parallel. Accordingly, the proposed method computed the $K/4$ -nearest neighbors of each simplex vertex independently on each GPU (see §5.3 for further discussion). The number of neighbors was chosen from $K/4 \in \{1, 2, 4, 8\}$.³ The weight β on the commitment loss (Equation 10) for STE-based methods (including SimVQ) and rotational gradient estimation was set to 1.0, following Fifty et al. (2025) and Zhu et al. (2025).

Table 1 reports the codebook utilization and reconstruction performance—including root mean squared error (rMSE), Inception Score (IS; Salimans et al., 2016), and Fréchet Inception Distance (FID; Heusel et al., 2017)—for the proposed method (“KNN-L2/CE”) and the baselines. Reconstruction quality deteriorated substantially when softmax-smoothed quantization (i.e., without Gumbel randomness) was combined with the perplexity-based regularization (“PPL”; Equation 11). This degradation arises from a mismatch between soft quantization during the training and hard quantization at inference; the smoothed quantizers deviated from the simplex vertices, as reflected by their high individual perplexity, $\exp(-\sum_{m=1}^M p_m \log p_m)$ (Table 2). These results support the argument made in the Introduction that perplexity-based regularization alone does not promote tight smoothing.

Perplexity-based regularization was effective only when combined with the Gumbel-softmax sampling, and onehot quantization in the forward pass via STE was necessary to ensure full codebook utilization (“Hard-Gumbel”). Without hard quantization, code collapse was not prevented at higher channel dimensionalities ($C \geq 32$; “Soft-Gumbel”).

By contrast, the proposed KNN-based regularization consistently prevented code collapse and achieved near-complete codebook utilization without resorting to Gumbel-softmax sampling. Reconstruction performance was also superior to, or competitive with, the Gumbel-softmax plus perplexity baseline across all feature map sizes.

The choice of deviation metric (L2 distance vs. cross-entropy, CE) did not exhibit a consistent global advantage. One notable exception occurred at extremely high channel dimensionality ($C = 2048$). In this regime, KNN-L2 failed to achieve full codebook utilization, whereas KNN-CE maintained complete utilization. Moreover, the soft quantizers under KNN-L2

²The exact implementation of \mathbf{p} and π involves normalization and rescaling; see Appendix A.1 for details.

³The value of K was upper-bounded at 8×4 by available computational resources; With a maximum batch size of 64, the total number of latent pixels was $64 \times 64 \times 64 = 8 \times 4 \times 8196$, allowing only 8×4 neighbors per vertex of Δ^{8196} . This implementation constraint is further discussed in §5.3.

Table 1: Performance of discrete autoencoding on the ImageNet validation set. Reported metrics are codebook usage and reconstruction quality scores: root mean squared error (rMSE), Fréchet Inception Distance (FID), and Inception Score (IS). The proposed method is denoted as “KNN-L2/CE”. Best scores across all methods are highlighted in boldface, while underlined values indicate the best-performing number of nearest neighbors among $K/4 \in \{1, 2, 4, 8\}$.

Method	$K/4$	16×16×32; 1024				Feature Map Size; Codebook Size				64×64×32; 8196				64×64×2048; 8196				
		Code Use (\uparrow)	rMSE (\downarrow)	FID (\downarrow)	IS (\uparrow)	Code Use	rMSE	FID	IS	Code Use	rMSE	FID	IS	Code Use	rMSE	FID	IS	
STE	Euclid	—	4.5%	0.404	124.86	36.61	100.0%	0.167	7.25	402.84	1.7%	0.235	22.02	290.24	0.1%	0.274	32.60	227.73
	Cosine	—	3.0%	0.381	117.95	41.48	70.9%	0.197	13.97	348.31	2.8%	0.186	12.11	363.86	0.2%	0.227	23.03	290.15
	SimVQ	—	100.0%	0.340	87.26	71.33	100.0%	0.170	7.44	400.41	100.0%	0.148	3.97	436.29	70.8%	0.682	286.18	3.19
RE	Euclid	—	3.1%	0.460	170.30	19.25	78.85%	0.171	10.21	377.56	0.5%	0.271	40.58	203.52	0.1%	0.301	53.81	153.77
	Cosine	—	2.8%	0.423	157.77	24.33	99.5%	0.194	14.67	344.17	4.4%	0.180	10.83	372.89	1.3%	0.193	16.98	331.17
HG	PPL	—	100.0%	0.349	100.29	54.04	100.0%	0.189	19.07	321.16	100.0%	0.163	10.33	384.04	100.0%	0.165	8.89	392.77
	KNN-CE	1	100.0%	0.368	86.49	68.27	100.0%	0.226	14.27	342.64	100.0%	0.173	3.17	435.04	100.0%	0.177	3.42	432.08
SG	PPL	—	55.0%	0.826	173.59	9.61	100.0%	0.183	10.28	377.79	48.4%	0.386	45.61	167.14	34.6%	1.253	368.71	1.58
	KNN-CE	1	100.0%	0.569	194.74	16.60	100.0%	0.233	15.41	329.78	100.0%	0.186	3.83	425.33	100.0%	0.188	3.73	422.84
Softmax	PPL	—	100.0%	1.112	309.60	4.55	81.6%	0.701	37.99	196.72	99.8%	0.725	83.07	77.98	89.3%	1.345	84.52	80.39
	KNN-L2	1	100.0%	0.358	76.29	81.61	100.0%	0.224	12.08	354.36	100.0%	0.387	32.20	210.61	75.9%	1.259	104.22	56.87
		2	100.0%	0.366	81.69	71.75	100.0%	0.226	12.04	348.48	100.0%	0.175	3.62	427.42	58.3%	1.302	94.82	62.82
		4	100.0%	0.379	87.05	62.37	100.0%	0.205	9.01	383.56	100.0%	0.196	5.64	403.06	68.3%	1.283	96.45	73.56
		8	99.9%	0.343	73.72	88.53	100.0%	0.199	12.64	361.23	100.0%	0.204	7.91	381.65	80.8%	1.134	73.79	92.46
	KNN-CE	1	100.0%	0.366	79.80	74.69	100.0%	0.225	14.08	345.56	100.0%	0.175	2.81	437.72	100.0%	0.424	18.58	289.42
		2	100.0%	0.380	106.05	50.75	100.0%	0.227	14.34	338.37	100.0%	0.187	4.16	418.57	100.0%	0.212	4.22	416.56
		4	100.0%	0.748	255.59	9.03	100.0%	0.228	16.73	326.78	100.0%	0.204	6.98	387.88	100.0%	0.190	4.70	411.70
		8	100.0%	1.240	467.86	3.01	100.0%	0.219	14.24	343.23	100.0%	0.199	5.27	404.10	100.0%	0.201	3.77	416.71

Table 2: Tightness of softmax-based smoothing (without Gumbel sampling), measured by the individual perplexity of smoothed quantizers, $\exp(-\sum_{m=1}^M p_m \log p_m)$. Reported values are the 75th, 90th, and 99th percentiles, as well as the maximum, computed across all feature-map pixels in the ImageNet validation set.

Method	$K/4$	16×16×32; 1024				Feature Map Size; Codebook Size				64×64×32; 8192				64×64×2048; 8192			
		75%	90%	99%	Max	75%	90%	99%	Max	75%	90%	99%	Max	75%	90%	99%	Max
PPL	—	910.40	933.12	963.29	995.91	7559.89	7561.99	7563.10	7565.02	7230.60	7267.06	7315.62	7424.16	8191.71	8191.85	8192.02	8192.61
KNN-L2	1	1.17	1.59	2.36	6.26	1.00	1.00	1.00	4.00	2.24	40.45	86.53	249.64	8191.66	8191.82	8191.98	8192.34
	2	1.00	1.08	1.86	27.37	1.00	1.00	1.06	4.65	1.14	1.55	2.33	7.92	8191.49	8191.72	8191.94	8192.35
	4	1.00	1.06	1.86	62.99	1.00	1.00	1.00	4.61	1.00	1.06	1.80	20.42	8191.63	8191.80	8191.97	8192.36
	8	1.00	1.10	1.90	120.68	3.33	3.87	5.22	12.03	1.00	1.05	1.79	107.70	8191.69	8191.82	8191.97	8192.41
KNN-CE	1	1.18	1.60	2.38	6.28	3.96	4.51	5.81	11.96	1.09	1.45	2.17	5.94	1.90	124.24	503.28	1024.38
	2	1.23	1.72	2.73	8.07	4.04	4.66	6.16	11.77	1.06	1.38	2.08	6.15	1.28	2.24	16.83	676.31
	4	1.42	1.78	2.38	5.45	4.16	4.86	6.57	13.04	1.08	1.44	2.16	6.58	1.36	1.98	3.16	11.94
	8	2.38	2.80	3.71	7.78	4.46	5.31	7.39	13.81	1.29	1.75	2.65	9.26	1.86	2.51	4.28	26.69

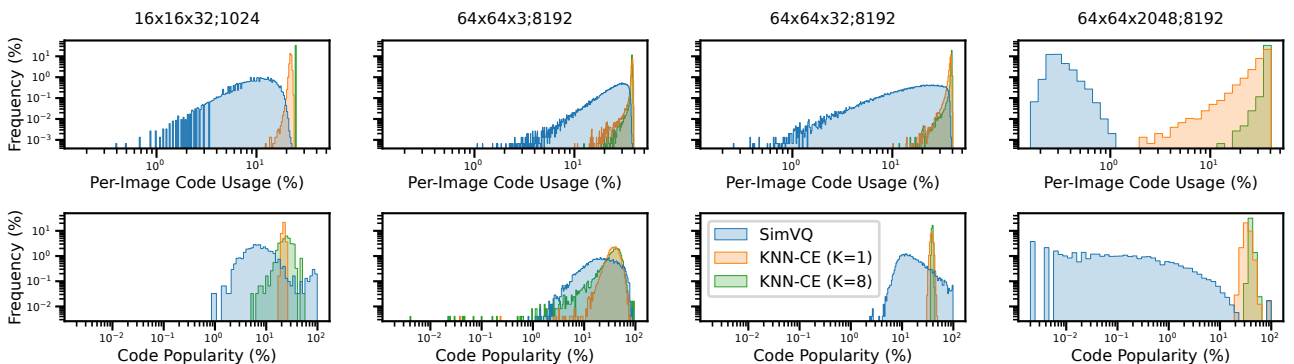


Figure 2: (Top) Histogram of per-image codebook utilization on the validation dataset, defined as the percentage of codes used at least once within each image. (Bottom) Histogram of code popularity, measured as the proportion of validation images that contain each code.

Table 3: Codebook usage in Wav2Vec 2.0 pretraining, evaluated on the LibriSpeech dev-clean split (similar results were observed for the other dev/test splits).

Method	$K/4$	#Codebooks \times Codebook Size	
		1 \times 1024	2 \times 320
STE	Euclid	—	0.8%
	Cosine	—	0.2%
	SimVQ	—	0.2%
RE	Euclid	—	2.5%
	Cosine	—	0.2%
HG	PPL	—	0.7%
	KNN-L2	2	0.2%
	KNN-CE	2	99.7%
SG	PPL	—	0.3%
	KNN-L2	2	90.1%
	KNN-CE	2	100.0%
Softmax	PPL	—	0.2%
	KNN-L2	1	82.4%
		2	60.4%
	KNN-CE	1	99.5%
		2	100.0%

failed to concentrate around the simplex vertices in the high-dimensionality condition, as indicated by their near-maximal individual perplexity values (Table 2). This looseness in smoothing also led to degraded reconstruction quality (Table 1).

Cross-entropy was additionally favorable in terms of computational efficiency. Its performance was highest when using the minimum number of neighbors ($K/4 = 1$) for nearly all feature map sizes (underlined entries in Table 1); increasing K yielded no further gains except in the extreme case of $C = 2048$. Although most soft quantizers remained formally unregularized under this setting, they nonetheless achieved low individual perplexity after training (Table 2), indicating a tight approximation to hard quantization. By contrast, minimizing the L2 distance to only a single nearest neighbor per GPU led to performance degradation for feature maps of size $64 \times 64 \times \{32, 2048\}$. Because increasing the number of neighbors requires a larger batch size (see §5.3 for details), cross-entropy emerges as the more scalable option.

Finally, both STE and rotational gradient estimation (RE) exhibited severe code collapse at higher channel dimensionalities ($C \geq 32$), reaffirming prior findings that reducing channel dimensionality is critical for stable training (Yu et al., 2022a, 2024; Mentzer et al., 2024). SimVQ was more robust, maintaining full codebook utilization and strong reconstruction performance at $C = 32$. However, when the channel dimensionality increased to $C = 2048$, its performance fell below that of classical STE-based models. Although SimVQ still utilized 70.8% of the codebook overall, each individual image was encoded by using no more than 1% of the codes (Figure 2). Effective vector quantization instead requires diverse code usage within individual images (typically 10–40%), a property that KNN-CE regularization preserves across channel dimensionalities ($C \in \{3, 32, 2048\}$).

The next section presents a case study in which all gradient-estimation approaches—including SimVQ—exhibit more pronounced code collapse, highlighting the difficulty of achieving robust prevention of code collapse across different settings.

4.2 Contrastive Learning

The second experiment evaluated vector quantization methods within Wav2Vec 2.0 pretraining for speech feature extraction (Baevski et al., 2020b). Unlike autoencoding, this pretraining integrates vector quantization directly into the main loss function.

Two codebook configurations were investigated. The first used a single codebook of size 1024. By contrast, the second followed the original work of Baevski et al. (2020b), combining two smaller codebooks—each of size 320—to implement rich code diversity efficiently via *product quantization* (Jégou et al., 2011, see §5.3 for more information). The dimensionality of the codebook vectors was set to 256 for the single-codebook configuration and to 128 for the dual-codebook configuration. The weight β on the commitment loss in both STE (including SimVQ) and rotational gradient estimation was set to 1.0 (Fifty et al., 2025; Zhu et al., 2025).

Models were trained on the LibriSpeech dataset, combining all training splits (train-clean-100 + train-clean-360 + train-other-500; Panayotov et al., 2015). Further details on the network architecture and learning objective are provided in

Appendix B.2.

Table 3 reports codebook usage. The perplexity-based regularization failed to prevent code collapse in both single- and dual-codebook settings. Likewise, the STE and rotational gradient estimation approaches exhibited the same failure. Remarkably, SimVQ—despite achieving full codebook usage in the discrete autoencoding experiments—offered no observable benefit in this learning paradigm.

By contrast, the proposed KNN-based regularization ensured high code utilization in both conditions. As in the discrete autoencoding experiments, a single neighbor per GPU was sufficient to obtain this effect.

5 Discussions

5.1 Summary of Findings & Contributions

This study introduced a simple and unified regularization method that simultaneously tightens smoothed vector quantization and promote effective code utilization. The proposed method successfully prevented code collapse in two representative applications of vector quantization: a middle layer in discrete autoencoding (§4.1) and target construction in contrastive learning (§4.2). This robustness is noteworthy, as prior approaches were effective only in specific settings and remained vulnerable to code collapse in others.

The proposed method is geometrically intuitive and straightforward, yet appears unaddressed in the existing literature. Research on neural vector quantization has traditionally been rooted in variational autoencoding (Kingma and Welling, 2014), primarily aiming to extend this stochastic framework to discrete variables (Jang et al., 2017; van den Oord et al., 2017). The issue of code collapse was recognized (or documented) later, and workarounds were developed independently of the quantization methods themselves (Dieleman et al., 2018; Baevski et al., 2020b; Dhariwal et al., 2020).

By contrast, the present work reformulates neural vector quantization as a simple smoothing problem: onehot vectors are approximated by elements of the simplex. Within this perspective, concentrating the approximators near the simplex vertices naturally arises as a desirable property. This reformulation, together with the proposed regularization strategy, represents a key conceptual contribution of the study.

5.2 Alternative Implementations of the Intended Regularization

Alternative regularization strategies could also achieve the intended distribution of smoothed quantizers (\mathbf{p} or π) around the simplex vertices. For example, one could align smoothed quantizers with a Dirichlet distribution with concentration parameters $\alpha_1 = \dots = \alpha_K < 1.0$ (Figure 3). The probability density of such a distribution is highest at the vertices of the simplex, thus matching the ideal distribution of smoothed quantizers. A possible formalization of this alignment is based on the Kullback-Leibler (KL) divergence between the Dirichlet prior (\mathbb{P}) and the distribution inferred from smoothed quantizers (\mathbb{Q}).

$$\mathcal{D}_{\text{KL}}(\mathbb{P} \mid \mathbb{Q}) := \int_{\Delta^{M-1}} \mathbb{P}(\mathbf{p}) \log \frac{\mathbb{P}(\mathbf{p})}{\mathbb{Q}(\mathbf{p})} d\mathbf{p} \quad (14)$$

However, Equation 14 is difficult to use directly as a regularization loss, due to the complexity of estimating \mathbb{Q} from sample quantizers, \mathbf{p} . Although one could constrain \mathbb{Q} as another Dirichlet to make the KL divergence tractable, maximum likelihood estimation of its parameters requires iterative algorithms (e.g., the Newton-Raphson method; Ronning, 1989; Sklar, 2014; Wicker et al., 2008), complicating and slowing gradient-based optimization in deep learning frameworks. Moreover, this estimation involves digamma and trigamma functions (Sklar, 2014), whose derivatives can explode when the concentration parameters approach small values—as desired for tight smoothing—during the course of learning.

A more practical approach is to approximate Equation 14 itself in a tractable manner. For instance, Perez-Cruz (2008) proposed a KNN-based estimation of the KL divergence that relies solely on *samples* from the two distributions, using the k -th nearest neighbor from \mathbb{Q} for each sample from \mathbb{P} . The regularization method proposed in this study can thus be interpreted as minimizing this estimated KL divergence, with the samples from \mathbb{P} constrained to onehot vectors.

5.3 Limitations

A primary limitation of the proposed method is its memory requirement. When training across multiple GPUs, the KNN-based regularization identifies K nearest smoothed quantizers (\mathbf{p} or π) per simplex vertex *on each GPU*, rather than

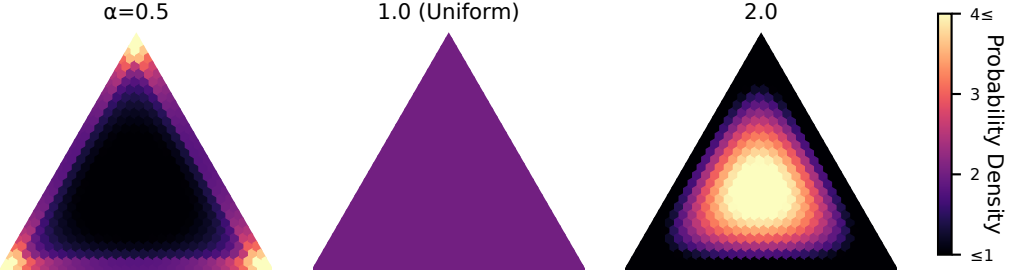


Figure 3: Dirichlet distributions on the simplex Δ^{3-1} with concentration parameters $\alpha_1 = \alpha_2 = \alpha_3 = \alpha$, where $\alpha \in \{0.5, 1.0, 2.0\}$.

finding global neighbors across all GPUs. Consequently, each GPU must have sufficient VRAM to store at least KM latent pixels/frames, where M denotes the codebook size. This requirement can become prohibitive when M is large (i.e., for fine-grained quantization), although empirically, a single neighbor per GPU appeared sufficient to prevent code collapse when cross-entropy was used as the divergence metric.

One possible workaround is to randomly select a subset of simplex vertices when computing the regularization loss, rather than using all vertices in a single iteration. In expectation, this achieves the same effect as the original implementation, although its empirical effectiveness remains to be assessed in future studies.

Additionally, fine-grained quantization can be achieved more efficiently using smaller G codebooks in combination (product quantization; Jégou et al., 2011), as explored in the Wav2Vec 2.0 pretraining (§4.2). This approach represents $\prod_{g=1}^G M_g$ distinct quantized vectors while requiring only $K \sum_{g=1}^G M_g$ smoothed quantizers per GPU. Leveraging these strategies, the proposed method can overcome its limitation and become applicable to real-world scenarios.

Acknowledgments

This study was supported by JSPS Grant-in-Aid for Scientific Research A (JP24H00774), B (JP22H03914), and C (JP-24K15087); JST AIP Accelerated Program (JPMJCR25U6) and Core Research for Evolutional Science and Technology (JPMJCR22P5); and Kayamori Foundation of Informational Science Advancement (K35XXVIII620). The author also gratefully acknowledges the support of the Academic Center for Computing and Media Studies, Kyoto University, regarding the use of their supercomputer system.

References

Baevski, A., Schneider, S., and Auli, M. (2020a). vq-wav2vec: Self-supervised learning of discrete speech representations. In *Proceedings of the 8th International Conference on Learning Representations (ICLR)*. OpenReview.net.

Baevski, A., Zhou, Y., Mohamed, A., and Auli, M. (2020b). wav2vec 2.0: A framework for self-supervised learning of speech representations. In Larochelle, H., Ranzato, M., Hadsell, R., Balcan, M. F., and Lin, H., editors, *Advances in Neural Information Processing Systems*, volume 33, pages 12449–12460. Curran Associates, Inc.

Chollet, F. (2017). Xception: Deep learning with depthwise separable convolutions. In *2017 IEEE Conference on Computer Vision and Pattern Recognition (CVPR)*, pages 1800–1807.

Deng, J., Dong, W., Socher, R., Li, L.-J., Li, K., and Fei-Fei, L. (2009). ImageNet: A large-scale hierarchical image database. In *2009 IEEE Conference on Computer Vision and Pattern Recognition*, pages 248–255.

Dhariwal, P., Jun, H., Payne, C., Kim, J. W., Radford, A., and Sutskever, I. (2020). Jukebox: A generative model for music.

Dieleman, S., van den Oord, A., and Simonyan, K. (2018). The challenge of realistic music generation: modelling raw audio at scale. In Bengio, S., Wallach, H., Larochelle, H., Grauman, K., Cesa-Bianchi, N., and Garnett, R., editors, *Advances in Neural Information Processing Systems*, volume 31. Curran Associates, Inc.

Esser, P., Rombach, R., and Ommer, B. (2021). Taming Transformers for high-resolution image synthesis. In *Proceedings of the IEEE/CVF Conference on Computer Vision and Pattern Recognition (CVPR)*, pages 12868–12878, Los Alamitos, CA, USA. IEEE Computer Society.

Fifty, C., Junkins, R. G., Duan, D., Iyengar, A., Liu, J. W., Amid, E., Thrun, S., and Ré, C. (2025). Restructuring vector quantization with the rotation trick. In *The Thirteenth International Conference on Learning Representations, ICLR 2025, Singapore, April 24-28, 2025*. OpenReview.net.

Gray, R. (1984). Vector quantization. *IEEE ASSP Magazine*, 1(2):4–29.

Hadjeris, G. and Crestel, L. (2020). Vector quantized contrastive predictive coding for template-based music generation.

He, K., Zhang, X., Ren, S., and Sun, J. (2016). Deep residual learning for image recognition. In *The IEEE Conference on Computer Vision and Pattern Recognition (CVPR)*, pages 770–778.

Heusel, M., Ramsauer, H., Unterthiner, T., Nessler, B., and Hochreiter, S. (2017). Gans trained by a two time-scale update rule converge to a local nash equilibrium. In Guyon, I., Luxburg, U. V., Bengio, S., Wallach, H., Fergus, R., Vishwanathan, S., and Garnett, R., editors, *Advances in Neural Information Processing Systems*, volume 30. Curran Associates, Inc.

Jang, E., Gu, S., and Poole, B. (2017). Categorical reparameterization with Gumbel-softmax. In *Proceedings of the 5th International Conference on Learning Representations (ICLR)*.

Jégou, H., Douze, M., and Schmid, C. (2011). Product quantization for nearest neighbor search. *IEEE Transactions on Pattern Analysis and Machine Intelligence*, 33(1):117–128.

Kingma, D. P. and Welling, M. (2014). Auto-encoding variational bayes. The International Conference on Learning Representations (ICLR) 2014.

Mentzer, F., Minnen, D., Agustsson, E., and Tschannen, M. (2024). Finite scalar quantization: VQ-VAE made simple. In *Proceedings of the Twelfth International Conference on Learning Representations (ICLR)*. OpenReview.net.

Panayotov, V., Chen, G., Povey, D., and Khudanpur, S. (2015). Librispeech: An ASR corpus based on public domain audio books. In *2015 IEEE International Conference on Acoustics, Speech and Signal Processing (ICASSP)*, pages 5206–5210, South Brisbane, Queensland, Australia.

Perez-Cruz, F. (2008). Kullback-leibler divergence estimation of continuous distributions. In *2008 IEEE International Symposium on Information Theory*, pages 1666–1670.

Ramesh, A., Pavlov, M., Goh, G., Gray, S., Voss, C., Radford, A., Chen, M., and Sutskever, I. (2021). Zero-shot text-to-image generation. In Meila, M. and Zhang, T., editors, *Proceedings of the 38th International Conference on Machine Learning*, volume 139 of *Proceedings of Machine Learning Research*, pages 8821–8831. PMLR.

Rombach, R., Blattmann, A., Lorenz, D., Esser, P., and Ommer, B. (2022). High-resolution image synthesis with latent diffusion models. In *2022 IEEE/CVF Conference on Computer Vision and Pattern Recognition (CVPR)*, pages 10674–10685.

Ronning, G. (1989). Maximum likelihood estimation of dirichlet distributions. *Journal of Statistical Computation and Simulation*, 32(4):215–221.

Salimans, T., Goodfellow, I., Zaremba, W., Cheung, V., Radford, A., Chen, X., and Chen, X. (2016). Improved techniques for training GANs. In Lee, D., Sugiyama, M., Luxburg, U., Guyon, I., and Garnett, R., editors, *Advances in Neural Information Processing Systems*, volume 29. Curran Associates, Inc.

Sklar, M. (2014). Fast MLE computation for the dirichlet multinomial.

van den Oord, A., Vinyals, O., and Kavukcuoglu, K. (2017). Neural discrete representation learning. In Guyon, I., Luxburg, U. V., Bengio, S., Wallach, H., Fergus, R., Vishwanathan, S., and Garnett, R., editors, *Advances in Neural Information Processing Systems 30*, pages 6306–6315. Curran Associates, Inc.

Wicker, N., Muller, J., Kalathur, R. K. R., and Poch, O. (2008). A maximum likelihood approximation method for dirichlet's parameter estimation. *Computational Statistics & Data Analysis*, 52(3):1315–1322.

Yu, J., Li, X., Koh, J. Y., Zhang, H., Pang, R., Qin, J., Ku, A., Xu, Y., Baldridge, J., and Wu, Y. (2022a). Vector-quantized image modeling with improved VQGAN. In *Proceedings of the International Conference on Learning Representations (ICLR)*.

Yu, J., Xu, Y., Koh, J. Y., Luong, T., Baid, G., Wang, Z., Vasudevan, V., Ku, A., Yang, Y., Ayan, B. K., Hutchinson, B., Han, W., Parekh, Z., Li, X., Zhang, H., Baldridge, J., and Wu, Y. (2022b). Scaling autoregressive models for content-rich text-to-image generation. *Transactions on Machine Learning Research*.

Yu, L., Lezama, J., Gundavarapu, N. B., Versari, L., Sohn, K., Minnen, D., Cheng, Y., Gupta, A., Gu, X., Hauptmann, A. G., Gong, B., Yang, M., Essa, I., Ross, D. A., and Jiang, L. (2024). Language model beats diffusion - tokenizer is key to visual generation. In *The Twelfth International Conference on Learning Representations, ICLR 2024, Vienna, Austria, May 7-11, 2024*. OpenReview.net.

Zhu, Y., Li, B., Xin, Y., Xia, Z., and Xu, L. (2025). Addressing representation collapse in vector quantized models with one linear layer. In *Proceedings of the IEEE/CVF International Conference on Computer Vision (ICCV)*, pages 22968–22977.

A Implementation of the Quantization Methods

This section provides details on the implementation of the quantization methods.

A.1 Smoothed Quantization

Smoothed quantizers \mathbf{p} were computed as $\mathbf{p} = \text{softmax}(\hat{Q}^\top \hat{\mathbf{z}}/t)$. In other words, the codebook vectors $(\mathbf{q}_1, \dots, \mathbf{q}_M) = Q$ and the feature vectors \mathbf{z} were first L2-normalized, and their product (i.e., cosine similarity) was rescaled by a learnable temperature t . This temperature was shared across the codebook so that all the logits had the same amplitude. Assignment probabilities π for Gumbel-softmax sampling were computed in the same way, while the additional temperature parameter— τ in Equation 7—was fixed as 1.0.⁴

A.2 Hard Quantization

The weight β on the commitment loss in Equation 10 was set to 1.0 (Fifty et al., 2025; Zhu et al., 2025), based on the previous observations that its value does not significantly affect learning outcomes within the range 0.1–2.0. (van den Oord et al., 2017).

B Details of the Experiments

B.1 Discrete Autoencoding

This section provides implementation details for the autoencoding experiment described in §4.1.

The network architecture followed prior work on discrete autoencoding of ImageNet (Esser et al., 2021; Fifty et al., 2025). Input images were center-cropped to $H \times W \times C = 256 \times 256 \times 3$. The encoder first expanded the channel dimensionality of the input images from 3 to 256 by convolution, and then progressively downsampled them through a series of strided convolutions (see Table 4 for the spatial and channel sizes at each layer). Each downsampling layer was followed by a residual block (He et al., 2016). The decoder reconstructed the input images by upsampling the latent feature maps with a sequence of interpolations and residual blocks.

To improve memory efficiency—particularly important for the proposed KNN-based regularization—all but the input and output layers were implemented as depthwise separable convolutions (Chollet, 2017). All convolutional kernels had size 3×3 .

Training employed the AdamW optimizer with $(\beta_1, \beta_2) = (0.9, 0.99)$ and a weight decay coefficient of 10^{-4} , except for Euclidean-based STE/rotational hard quantization, where weight decay was set to zero. The learning rate was linearly warmed up from 0.0 to ρ_{\max} , and subsequently annealed to $0.5\rho_{\max}$ by cosine scheduling. The maximum learning rate ρ_{\max} was set to 5×10^{-5} for Euclidean-based STE/rotational hard quantization, and to 10^{-4} for all other configurations (Fifty et al., 2025).

Inception Score (IS; Salimans et al., 2016) and Fréchet Inception Distance (FID; Heusel et al., 2017) were estimated using the ImageNet-pretrained Inception V3 provided in torchvision.

⁴Previous studies manually annealed the Gumbel-softmax temperature from $\tau = 0.5$ to 2.0, scaling it by 0.999995 at each iteration (Baevski et al., 2020b). This approach was also tested in the experiments here but did not yield improvements over the fixed temperature.

Table 4: Hyperparameters for discrete autoencoding.

Feature Map Size	16 × 16 × 32	64 × 64 × 3	64 × 64 × 32	64 × 64 × 2048
Codebook Size	1024	8196	8196	8196
Latent Channels	128 → 128 → 64 → 64 → 32 → 32		128 → 64 → 32 → {3, 32, 2048}	
Height & Width	256 → 128 → 64 → 32 → 16 → 16		256 → 128 → 64 → 64	
Batch Size	64	64	64	64
Training Epochs	25	25	20	20
Warmup Iterations	16,000	16,000	16,000	16,000

Table 5: Hyperparameters for Wav2Vec 2.0.

Input Frequency	16kHz
Latent Frequency	50Hz
Codebook Dimensionality	256
Codebook Size	1024
CNN	
Latent Channels	512
Kernel Sizes	10→3→3→3→3→2→2
Strides	5→2→2→2→2→2
Transformer	
# Layers	12
Model Dimensionality	768
# Heads	8
Feed-Forward Dimensionality	4096
Dropout Rate	0.1
Layer Drop	0.05
	#Codebooks×Codebook Size
	1×1024 2×320
Batch Size	128 64
Training Epochs	128 20
Warmup Iterations	32,000 10,000

B.2 Wav2Vec 2.0

This section provides details for the Wav2Vec 2.0 pretraining discussed in §4.2.

The model consisted of a convolutional feature encoder followed by a Transformer module (Baevski et al., 2020b). The convolutional encoder extracted latent feature sequences from input waveforms (16kHz→50Hz). Then, a subset of these latent vectors was masked and fed into the Transformer, whose outputs \mathbf{y}_t were trained to predict the quantized version \mathbf{q}_t of the masked vectors. The masking scheme followed Baevski et al. (2020b); random 6.5% of the latent vectors were masked, together with the following 10 time steps. The learning objective was:

$$\mathcal{L}_{\text{main}} = -\log \frac{\exp(\hat{\mathbf{y}}_t \hat{\mathbf{q}}_t^\top / \mathcal{T})}{\sum_{\tilde{\mathbf{q}} \sim Q} \exp(\hat{\mathbf{y}}_t \tilde{\mathbf{q}}^\top / \mathcal{T})} \quad (15)$$

where $\hat{\cdot}$ denotes the L2-normalization of vectors (i.e., measuring the cosine similarity), and $\mathcal{T} := 0.1$ is the temperature parameter. For each masked vector, a set of distractors $\tilde{\mathbf{q}}$ was sampled from the other quantized vectors according to a distribution Q .

Both the convolutional encoder and Transformer were implemented using the publicly available code in torchaudio, and only the quantization module was implemented from scratch.

Input waveforms were randomly cropped to the length of 250k samples. Both stages employed the AdamW optimizer with $(\beta_1, \beta_2) = (0.9, 0.99)$ and zero weight decay. The learning rate was warmed up from 0.0 to 5.0×10^{-4} , and then annealed to 5.0×10^{-6} by cosine scheduling.

When the single-codebook condition was first examined, training was run for 128 epochs, following the original schedule (Baevski et al., 2020b). However, since convergence occurred rapidly, the number of epochs was reduced in the dual-codebook condition to improve time efficiency.